The Astrophysical Journal, 711:417–423, 2010 March 1 doi:10.1088/0004-637X/711/1/417

GLOBAL SPECTRAL ENERGY DISTRIBUTION OF THE CRAB NEBULA IN THE PROSPECT OF THE *PLANCK* SATELLITE POLARIZATION CALIBRATION

J. F. Macías-Pérez[1], F. Mayet[1], J. Aumont[1], and F.-X. Désert[2]
[1] LPSC, Université Joseph Fourier Grenoble 1, CNRS/IN2P3, Institut National Polytechnique de Grenoble, 53, av. des Martyrs, 38026 Grenoble, France
[2] Laboratoire d'Astrophysique, Obs. de Grenoble, BP 53, 38041 Grenoble Cedex 9, France
Received 2009 October 6; accepted 2010 January 21; published 2010 February 10

ABSTRACT

Within the framework of the *Planck* satellite polarization calibration, we present a study of the Crab Nebula spectral energy distribution (SED) over more than six decades in frequency ranging from 1 to 10^6 GHz (from 299 to 2.99×10^{-4} mm). The *Planck* satellite mission observes the sky from 30 to 857 GHz (from 9.99 to 0.3498 mm) and therefore we focus on the millimeter region. We use radio and submillimeter data from the *WMAP* satellite between 23 and 94 GHz (from 13 to 3.18 mm), from the Archeops balloon experiment between 143 (2.1 mm) and 545 GHz (0.55 mm), and a compendium of other Crab Nebula observations. The Crab SED is compared to models including three main components: synchrotron that is responsible for the emission at low and high frequencies, dust that explains the excess of flux observed by the *IRAS* satellite, and an extra component on the millimeter regime. From this analysis, we conclude that the unpolarized emission of the Crab Nebula at microwave and millimeter wavelengths is the same synchrotron emission as the one observed in the radio domain. Therefore, we expect the millimeter emission of the Crab Nebula to be polarized with the same degree of polarization and orientation as the radio emission. We set upper limits on the possible errors induced by any millimeter extra component on the reconstruction of the degree and angle of polarization at the percent level as a maximum. This result strongly supports the choice by the *Planck* collaboration of the Crab Nebula emission for performing polarization cross-checks in the range 30 (299 mm) to 353 GHz (0.849 mm).

Key words: cosmic background radiation – cosmology: observations

Online-only material: color figures

1. INTRODUCTION

As the strongest source of synchrotron radiation in our Galaxy, the pulsar-powered Crab Nebula (Taurus A) is a well-studied astrophysical object and it is therefore used for calibration purpose. This will be the case for the *Planck* satellite mission which will use the Crab Nebula for polarization cross-checks in the frequency range from 30 to 353 GHz. A good understanding of the spectral energy distribution (SED) of the source as well as of the total intensity flux within the *Planck* beam will be required for an accurate determination of the angle of polarization of the detectors and of a possible cross polarization effect between detectors as they limit the accuracy to which the cosmic microwave background (CMB) polarized angular power spectra will be measured.

The emission spectrum of the A.D. 1054 supernova remnant (SNR) has been the subject of a host of investigations over several decades in frequency. The radio spectrum is known to exhibit a synchrotron power law with a spectral index $\beta \simeq -0.299 \pm 0.009$ (Baars et al. 1977). This continuum from radio synchrotron seems to be fading with a rate $\alpha = (-0.167 \pm 0.015)\%$ yr^{-1} (Aller & Reynolds 1985). At higher frequency, above 10^4 GHz, the observation is also consistent with synchrotron emission with a power law of spectral index -0.73 (Véron-Cetty & Woltjer 1993).

The data from *IRAS* satellite Marsden et al. (1984) have been reanalyzed by Strom & Greidanus (1992) revealing a significant excess of emission over the low-frequency synchrotron spectrum, well explained by a single dust component at a temperature $T \sim 46$ K, thus requiring a 0.02 $M_\odot$ dust mass. Using MPifrR bolometer arrays at the IRAM 30 m telescope, Bandiera et al. (2002) gave the first evidence for a new component at millimeter wavelengths. They have shown that this 1.3 mm (230 GHz) excess flux cannot be interpreted as emission from a dust component whereas the data may be consistent with a low energy cutoff in the energy distribution of the emitting particles. However, at 847 μm (353 GHz) Green et al. (2004) found a good agreement with the canonical radio synchrotron emission and hence no need for an extra component. As the *Planck* satellite mission will use the Crab Nebula emission to perform polarization cross-check in the range 30–353 GHz, a deep knowledge of the physical origin of this emission is needed.

For this purpose, we use observations of the Crab Nebula by the *Wilkinson Microwave Anisotropy Probe* (*WMAP*) satellite at 23, 33, 41, 61, and 94 GHz (Page et al. 2007) and by the Archeops balloon experiment at 143, 217, 345, and 545 GHz (Macías-Pérez et al. 2007; Desert et al. 2008). These data in addition to already published ones are used to study the Crab Nebula SED. This paper is organized as follows. In Section 2, we present the reanalysis of the Archeops and *WMAP* data. Section 3 presents the SED of the Crab Nebula from 1 to 10^6 GHz and compares it to a model including the synchrotron and dust well-known components. In Section 4, we perform a coherent analysis of the Crab SED over the full frequency range adding an extra component to the previous model to account for the possible millimeter excess. The implications of our results for the *Planck* polarization calibration are discussed in Section 5. Summary and conclusions are given in Section 6.

2. REANALYSIS OF THE ARCHEOPS AND *WMAP* OBSERVATIONS

In this paper, we are mainly interested in the microwave and millimeter regimes for which the best currently available data

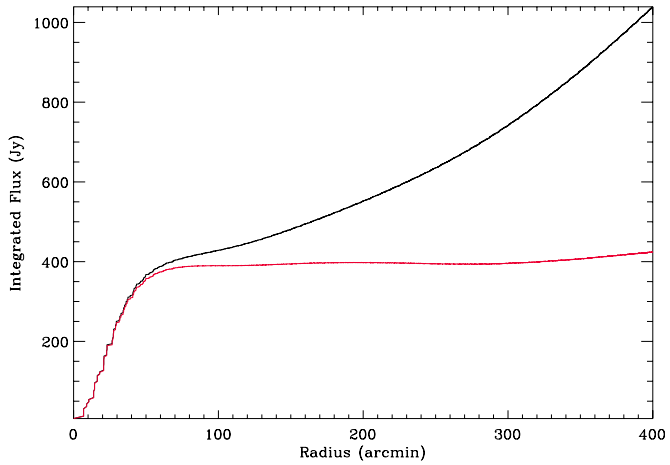

Figure 1. Integrated flux at 23 GHz as a function of the angular distance to the Crab Nebula center before (black) and after (red) background subtraction.
(A color version of this figure is available in the online journal.)

are the *WMAP* (Page et al. 2007) and Archeops (Desert et al. 2008) data. To avoid any bias on our analysis by a difference of treatment of these two data sets, we have decided to re-estimate the Crab Nebula unpolarized emission from 23 to 545 GHz using the publicly available *WMAP* (Page et al. 2007; Hinshaw et al. 2009) and Archeops (Macías-Pérez et al. 2007) intensity maps. Furthermore, to make the full data set as homogeneous as possible, the total intensity flux for each frequency was estimated using standard radial photometry techniques to mimic the flux integration performed for the high-resolution data sets. Note that we integrate far from the radio extension of the Crab Nebula, ∼5 arcmin radius, to recover the Crab Nebula flux diluted over the entire beam pattern. Therefore, a key issue for this analysis is the subtraction of the background galactic emission which is mainly due to synchrotron and free–free emissions at low frequencies and dust at high frequencies. As the *WMAP* and Archeops maps are available on Healpix format, we have developed our own radial photometry software for this pixelization scheme.

The results of this analysis are presented in Table 1. For Archeops, we obtain similar values to those in Desert et al. (2008) with slightly different error bars. However, for *WMAP*, we obtain values 8% larger than those in Page et al. (2007). Most probably the difference comes from the way the background subtraction is performed and the fact that the *WMAP* team computed the intensity and polarization simultaneously. It is important to stress that the difference with respect to the *WMAP* team is within the 1σ error bars at high frequency and goes up to 3σ at 23 GHz. To illustrate the problem of background subtraction, we show in Figure 1 the radial profile centered at the Crab Nebula position before (black) and after (red) background subtraction at 23 GHz. For this paper, we use our own estimation of the Crab Nebula flux in intensity but we have noticed that the final conclusions are not changed significantly by the choice of data set.

3. SED OF THE CRAB NEBULA

In this section, we present a coherent analysis of the Crab SED in the range 1–10^6 GHz based on a compendium of observations shown in Table 1. Note that to be able to directly compare to the Archeops and *WMAP* data, we have chosen only those data sets for which integrated fluxes over the full extension of the Crab Nebula are available.

Table 1
Compendium of Crab Nebula Observations from 1 to 10^6 GHz

ν (GHz)	S_ν (Jy)	ΔS_ν (Jy)	Central Epoch	Reference
1.117	990.0	59.4	1969.9	Vinogradova et al. (1971)
1.304	980.0	58.8	1969.9	Vinogradova et al. (1971)
1.4	930.0	46.5	1963	Kellermann et al. (1969)
1.765	940.0	56.4	1969.9	Vinogradova et al. (1971)
2.0	840.0	50.4	1969.3	Dmitrenko et al. (1970)
2.29	810.0	48.6	1969.3	Dmitrenko et al. (1970)
2.74	795.0	47.7	1969.3	Dmitrenko et al. (1970)
3.15	700.0	24.5	1964.4	Medd (1972)
3.38	718.0	43.1	1969.3	Dmitrenko et al. (1970)
3.96	646.0	38.8	1969.3	Dmitrenko et al. (1970)
4.08	687.0	20.6	1964.8	Penzias & Wilson (1965)
5.0	680	34	1963	Kellermann et al. (1969)
6.66	577.2	20.2	1965.	Medd (1972)
8.25	563.0	22.5	1965.9	Allen & Barrett (1967)
13.49	524.0	19.9	1969.9	Medd (1972)
15.5	461	24	1965.9	Allen & Barrett (1967)
16.0	447.0	15.6	1970.6	Wrixon et al. (1972)
22.285	397	16.0	1973.1	Janssen et al. (1974)
22.5	395	7	2003	This paper
31.41	387	72	1966.7	Hobbs et al. (1968)
32.8	340	5	2003	This paper
34.9	340	68	1967.3	Kalaghan & Wulfsberg (1967)
40.4	323	8.0	2003	This paper
60.2	294	10.0	2003	This paper
92.9	285	16.0	2003	This paper
111,1	290	35	1973.5	Zabolotnyi et al. (1976)
143	231	32	2002	This paper
217	182	38	2002	This paper
230	260	52	2000	Bandiera et al. (2002)
250	204	32	1985.3	Mezger et al. (1986)
300	194.0	19.4	1983	Chini et al. (1984)
300	131	42	1978.75	Wright et al. (1979)
300	300	80	1976.0	Werner et al. (1977)
347	190	19	1999.8	Green et al. (2004)
353	186	34	2002	This paper
545	237	68	2002	This paper
750	158	63	1978.75	Wright et al. (1979)
1000	135	41	1978.75	Wright et al. (1979)
3000	184	13	1983.5	Strom & Greidanus (1992)
5000	210	8	1983.5	Strom & Greidanus (1992)
12×10^3	67	4	1983.5	Strom & Greidanus (1992)
25×10^3	37	1	1983.5	Strom & Greidanus (1992)
3.246×10^5	6.57	0.66	1989	Véron-Cetty & Woltjer (1993)
4.651×10^5	4.78	0.48	1989	Véron-Cetty & Woltjer (1993)
5.593×10^5	4.23	0.42	1989	Véron-Cetty & Woltjer (1993)
7.878×10^5	3.22	0.32	1989	Véron-Cetty & Woltjer (1993)

Notes. Fluxes (S_ν) are presented in Jy. For Véron-Cetty & Woltjer (1993) and Chini et al. (1984), a conservative 10% error has been chosen to account for extrapolation errors. The central epoch of observation is also indicated. This is used for the evaluation of the fading effect of the low-frequency synchrotron component up to 100 GHz. Data values labeled in this paper for Archeops and *WMAP* are revaluated using the method described in Section 2.

3.1. Low-frequency Synchrotron Emission

An accurate determination of the low-frequency synchrotron component is necessary to assess the synchrotron contribution at millimeter frequencies. Any inter-comparison of low-frequency radio observations of the Crab Nebula must take into account its well-known secular decrease. In particular, Aller & Reynolds (1985) have estimated a secular decrease in the flux density at a rate $\alpha = (-0.167 \pm 0.015)\%$ yr^{-1} from observations at 8 GHz over the period 1968 to 1984. This result is in good

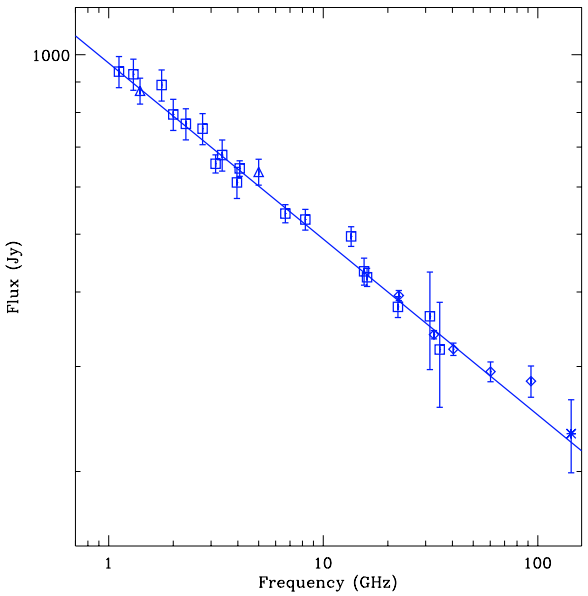

Figure 2. SED of the Crab Nebula from 1 to 100 GHz. Data samples are represented together with the best-fit power-law model to the data (see the text for details).

(A color version of this figure is available in the online journal.)

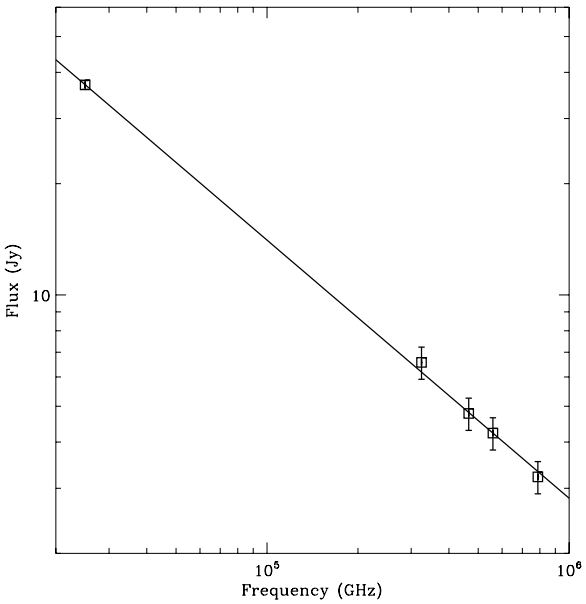

Figure 3. High-frequency SED of the Crab Nebula. Data samples are represented together with the best-fit power-law model to the data (see the text for details).

agreement with other studies at lower frequencies: for example, $\alpha = (-0.18 \pm 0.1)\%$ yr^{-1} over the period from 1977 to 2000 at 927 MHz by Vinyajkin (2005).

All these measurements are in fair agreement with theoretical evaluations of the evolution of pulsar-driven SNRs by Reynolds & Chevalier (1984) which predicts α ranging from -0.16% yr^{-1} to -0.4% yr^{-1}.

In this paper, the value $\alpha = -0.167\%$ yr^{-1} is chosen for the fading of the Crab Nebula and all data are converted to a common observation date, 2003 January 1. In Figure 2, we trace the flux of the Crab Nebula as a function of frequency for the fading corrected low-frequency data in Table 1 ranging from 1 to 143 GHz.

We observe a large decrease of flux with increasing frequency which can be represented by a power law of the form $A_1\left(\frac{\nu}{1\,\mathrm{GHz}}\right)^{\beta_1}$. By χ^2 minimization, we obtain for the low-frequency data up to 100 GHz

$$\beta_1 = -0.296 \pm 0.006 \quad \text{and} \quad A_1 = (973 \pm 19)\,\mathrm{Jy}$$

with $\chi^2/N_{\mathrm{dof}} = 1.03$ and this model is shown as a solid line in Figure 2. This result is in agreement with the "canonical" value $\beta \simeq -0.299 \pm 0.009$ from Baars et al. (1977)[3] at the 1σ level.

3.2. High-frequency Synchrotron and Dust Emission

The Crab synchrotron emission described above evolves at higher frequencies, around 10^4 GHz, toward a much harder SED with a spectral index of ~ -0.73 (see, for example, Véron-Cetty & Woltjer 1993). To accurately estimate the synchrotron emission properties at high frequency, we have fitted the data from 10^4 to 10^6 GHz presented in Table 1 to a power law of the form $A_2\nu^{\beta_2}$. By χ^2 minimization, we found the data to be well fitted, $\chi^2/N_{\mathrm{dof}} = 0.155$, by a power law of parameters

$$\beta_2 = (-0.698 \pm 0.018) \text{ and } A_2 = (43.5 \pm 8.8) \times 10^3\,\mathrm{Jy}.$$

[3] Kovalenko et al. (1994) obtained $\beta_1 = (-0.27 \pm 0.04)$.

Figure 3 represents the high-frequency data, and the best-fit power-law model is overplotted.

Finally, the infrared satellite observatory *IRAS* has revealed significant excess emission above this synchrotron contribution around 50 μm (Marsden et al. 1984). As shown by Strom & Greidanus (1992), this can be explained, after careful removal of the synchrotron component, by a single dust component described by a modified blackbody of emissivity $\beta = 2$ at $T = 46 \pm 3$ K, requiring a dust mass of 0.02 $M_\odot$.

3.3. Millimetric Excess

To evaluate a possible millimetric excess of flux in the range 100–1000 GHz, we assume the above canonical modeling of the Crab Nebula SED: a synchrotron component with a spectral index break at high frequency and a dust component at infrared wavelengths. We can thus reconstruct the Crab Nebula emission at the millimetric frequencies and compare it to the data in Table 1. Figure 4 shows the residuals to the canonical model from 10 to 2×10^4 GHz. We observe that there is no significant excess of power in the millimetric regime from 100 to 1000 GHz except for the 545 GHz Archeops data sample which presents only a 1.5σ excess. Indeed, the χ^2/N_{dof} for the null hypothesis is 0.69.

4. REFINED MODELING

In the previous section, we have proved that the millimetric data in Table 1, from 100 to 1000 GHz, are compatible with the canonical model assuming single synchrotron and dust components. However, it is interesting to check if an extra component may improve significantly the fit to the data. Following Bandiera et al. (2002), we consider either an extra low-temperature dust (LTD) emission or an extra synchrotron component. Thus, the three component models are defined as follows.

1. Canonical synchrotron that is described by four parameters: spectral index and amplitude for the low- and high-frequency emission. At high frequency, we consider both the amplitude and the spectral index fixed and set them to

Table 2
Best-fit Model Parameters and Errors for the Extra Dust Component Model

$\chi^2/N_{\rm dof}$	A_s (Jy)	A_D (Jy)	T_D (K)	β_D	$A_{\rm LTD}$ (Jy)	$T_{\rm LTD}$ (K)	$\beta_{\rm LTD}$	LTD %	$\chi^2_{mm}/N_{\rm dof}$
0.73	971 ± 9	128 ± 8	45.9 ± 1.2	1.93 ± 0.50	32 ± 24	5 ± 23	3.6 ± 2.4	26 ± 20	0.88

Notes. $\chi^2/N_{\rm dof}$ for the full data set and on the millimetric regime from 100 to 1000 GHz. LTD % stands for the percentage of flux at 545 GHz due to the extra dust component with respect to the total flux.

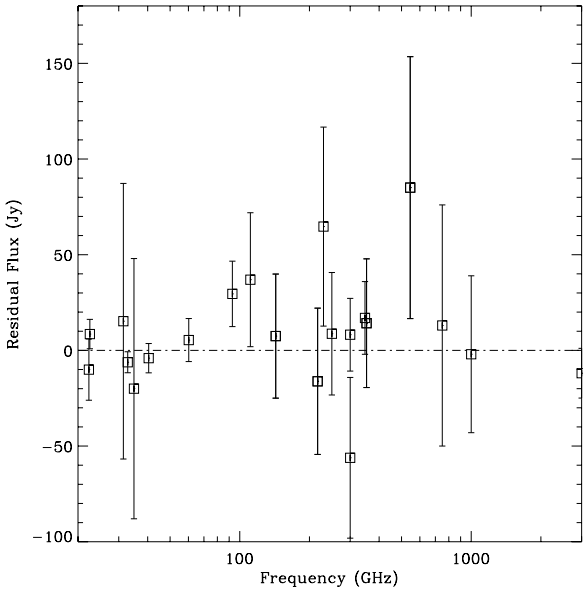

Figure 4. Residual to the standard model of the Crab Nebula emission assuming a synchrotron and a dust component in the range 10–2000 GHz (see the text for details). Note that the millimetric data were not used in the fit. We show the full data set in the region of interest.

the values obtained in Section 3.2. At low frequency, we fix the spectral index to the value obtained in Section 3.1 and the amplitude, A_S, is fitted. We also assume a constant fading of $\alpha = -0.167\%$ yr^{-1} as before.

2. Canonical dust (following Strom & Greidanus 1992) described by a modified blackbody with three free parameters A_D, T_D, and β_D that represent the amplitude, temperature, and spectral index, respectively.
3. One of the extra components as described below.

4.1. Extra Low-temperature Dust Emission

In Section 3.3, we concluded that at 545 GHz the difference between the standard model and the data is at its maximum. In the case of an extra dust component, this implies very low temperature dust in the range from 4 to 10 K. To model this component, we assume a modified blackbody spectrum with three free parameters $A_{\rm LTD}$, $T_{\rm LTD,}$ and $\beta_{\rm LTD}$ that represent the amplitude, temperature, and spectral index, respectively. The best-fit model to the data is found by χ^2 minimization on the full frequency range from 1 to 10^6 GHz.

Figure 5 presents on the left panel the observational data (black) and the global best-fit model to the data (red). The canonical synchrotron component is shown in light blue and the canonical dust in orange. The extra LTD component is represented in blue. The right panel presents the residuals to the best-fit model in the frequency range of interest. The parameters and error bars for the best-fit model to the data and the percentage of flux at 545 GHz associated with the extra component with respect to the total flux are given in Table 2. We also present the $\chi^2/N_{\rm dof}$ values for the global fit in the frequency range from 1 to 10^6 GHz and in the millimetric range from 100 to 1000 GHz.

We obtain a good global fit to the data as shown by the $\chi^2/N_{\rm dof}$ value. The best-fit parameters obtained for the canonical synchrotron and dust components are in good agreement with those presented in Section 3. Comparing with Strom & Greidanus (1992), we found the same dust temperature, 46 ± 1 K, with an error bar improved by a factor of 3, as we carefully account for the canonical synchrotron spectrum. The amplitude of the extra component is compatible with zero and therefore we conclude that there is no evidence for an extra component in the form of LTD. Furthermore, we observe that on the one hand the data require extremely low temperatures of 5 K with rather large error bars, therefore dust masses of $\sim 230\, M_\odot$, making the model rather unrealistic. On the other hand, the improvement of the $\chi^2/N_{\rm dof}$ in the millimetric region between 100 and 1000 GHz is not significant to justify the addition of the three extra parameters required by the LTD component. This is also clear on the right panel of Figure 5 where we represent the residuals to the best-fit model to the data on the millimetric regime.

4.2. Extra Synchrotron Component

For the extra synchrotron component, we consider, as in Bandiera et al. (2002), that the distribution of energy of the relativistic electrons responsible for the emission is well represented by a power law with spectral index in the range 1–3 and presents a low-energy cutoff. To account for an excess of flux in the millimeter regime, the critical frequency corresponding to the lowest energy electrons must be somewhere in the range 200–600 GHz. In total, the low-energy cutoff synchrotron (LECS) model has three parameters, p the spectral index of the electron energy distribution, ν_c the low-energy cutoff critical frequency, and $A_{\rm LECS}$ a normalization coefficient. The best fit to the data is found by χ^2 minimization.

The parameters and error bars of the best fit to the data for the three data sets as well as the percentage of flux due to the extra component with respect to the total flux at 545 GHz are given in Table 3. We also present $\chi^2/N_{\rm dof}$ values for the best fit to the data on the full data set from 1 to 10^6 GHz and on the millimetric regime from 100 to 1000 GHz. The left panel of Figure 6 presents the data in black and the global best-fit model to the data is represented in red. The canonical synchrotron component is shown in light blue and the canonical dust in orange. The extra LECS component is represented in blue.

As above, we obtain a good global fit to the data as shown by the $\chi^2/N_{\rm dof}$ value. The best-fit parameters obtained for the canonical synchrotron and dust components are in good agreement with those presented in Section 3 (Strom & Greidanus 1992). The amplitude of the extra synchrotron component is compatible with zero as well as the value of the spectral index of the electron energy distribution. We therefore conclude that there is no evidence of an extra component in the form of LECS.

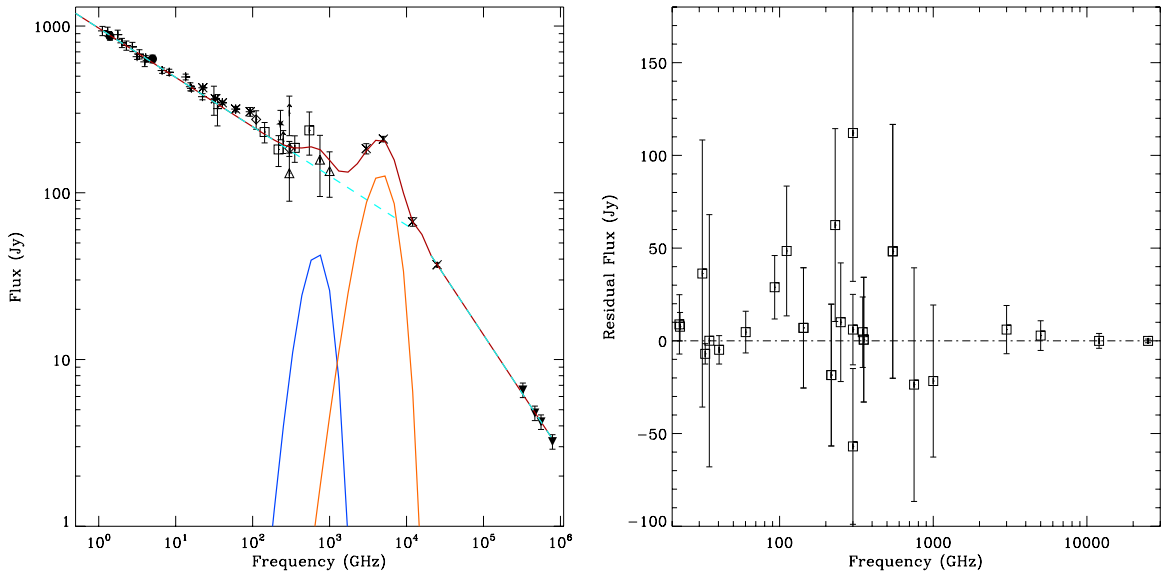

Figure 5. Refined modeling of the SED of the Crab Nebula in the frequency range from 1 to 10^6 GHz assuming an extra dust component at low temperature. Left panel: we represent the data from Table 1 (black), the best-fit model to the data (red) and the synchrotron (light blue), the main dust (orange) and the extra dust (dark blue) components associated with it. Right panel: residuals in the millimetric regime for the top panel models.

(A color version of this figure is available in the online journal.)

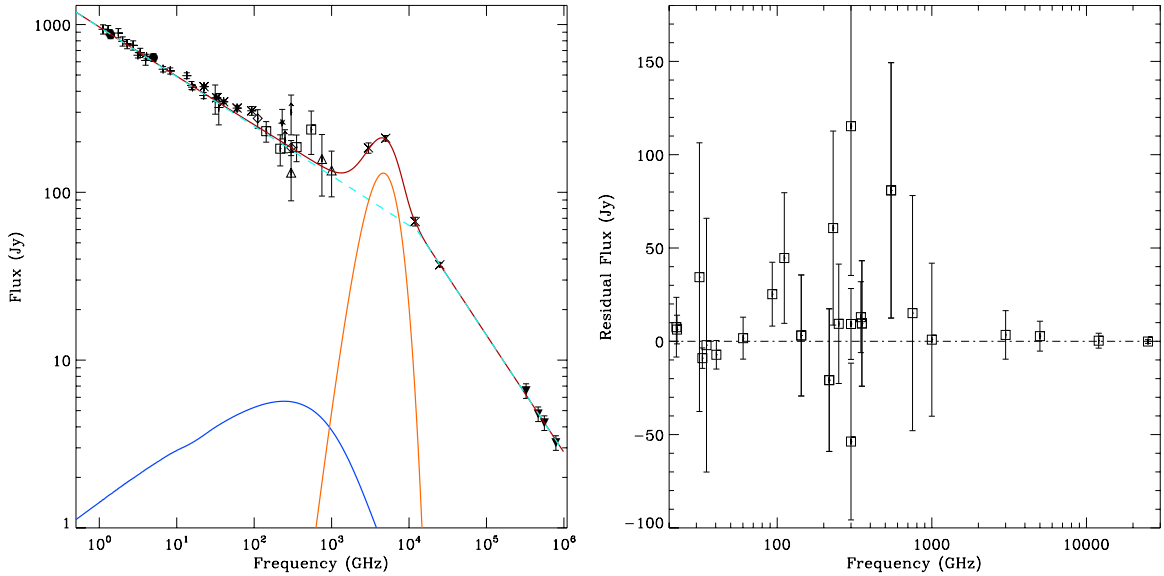

Figure 6. Refined modeling of the SED of the Crab Nebula in the frequency range from 1 to 10^6 GHz assuming an extra synchrotron component. Left panel: we represent the data from Table 1 (black), the best-fit model to the data (red) and the main synchrotron (light blue), the extra synchrotron (dark blue) and the dust components (orange) associated with it. Right panel: residuals in the millimetric regime for the top panel models.

(A color version of this figure is available in the online journal.)

Table 3
Best-fit Model Parameters and Errors for the Extra Synchrotron Component Model

$\chi^2/N_{\rm dof}$	A_s (Jy)	A_D (Jy)	T_D (K)	β_D	$A_{\rm LECS}$ (Jy)	ν_c (GHz)	p	LECS %	$\chi^2_{mm}/N_{\rm dof}$
0.76	965 ± 14	129 ± 9	46.0 ± 1.0	1.89 ± 0.4	5 ± 6	470 ± 317	3 ± 12	3 ± 3	0.93

Notes. $\chi^2/N_{\rm dof}$ for the full data set and on the millimetric regime from 100 to 1000 GHz. LECS % stands for the percentage of flux at 545 GHz due to the extra synchrotron component with respect to the total flux.

In addition, we observe that the $\chi^2/N_{\rm dof}$ in the millimetric region from 100 to 1000 GHz is worse than the one obtained in Section 3.3 assuming the canonical model only. The right panel of Figure 6 represents the residuals to the best-fit model to the data on the millimetric regime. From this, we conclude that the fit to the data in this frequency regime is not improved by adding an extra synchrotron component.

We have also performed the analysis of the data set considering the p and ν_c parameters fixed and set to the values quoted by Bandiera et al. (2002). The analysis shows that the amplitude of

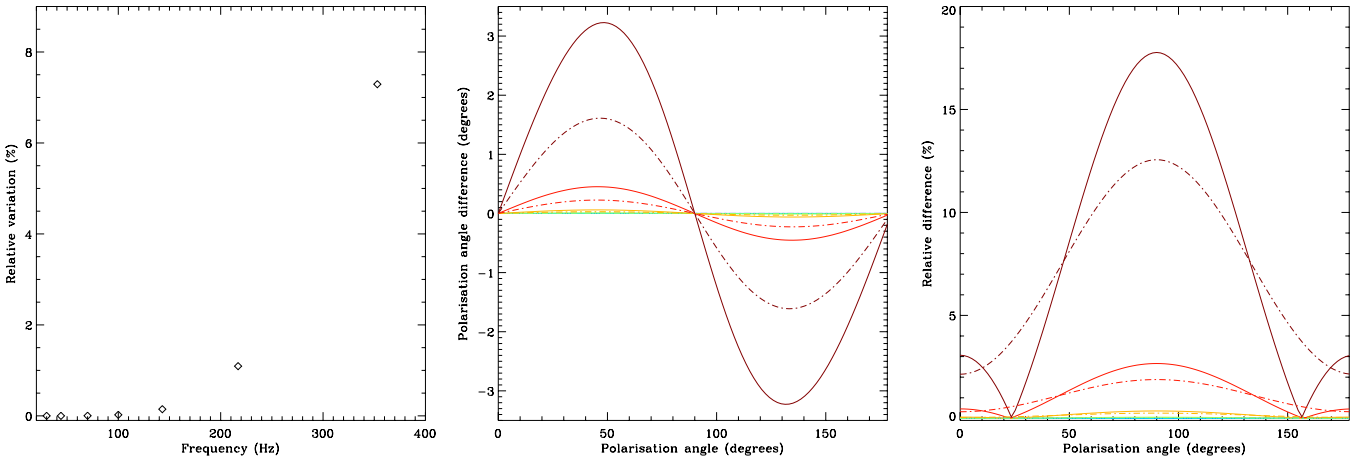

Figure 7. Errors induced in the degree and angle of polarization by an extra LTD component. Left plot: relative error on the degree of polarization in the case of an unpolarized extra component as a function of the frequency of the polarized *Planck* channels. Middle and right plots: relative error on the degree of polarization and polarization angle error in the case of an extra polarized component as a function of the polarization angle of this component. The dashed and solid lines correspond to an extra component with a degree of polarization of 5% and 10%, respectively. From blue to red, we represent the values for the different polarized *Planck* channels from 30 to 353 GHz.

(A color version of this figure is available in the online journal.)

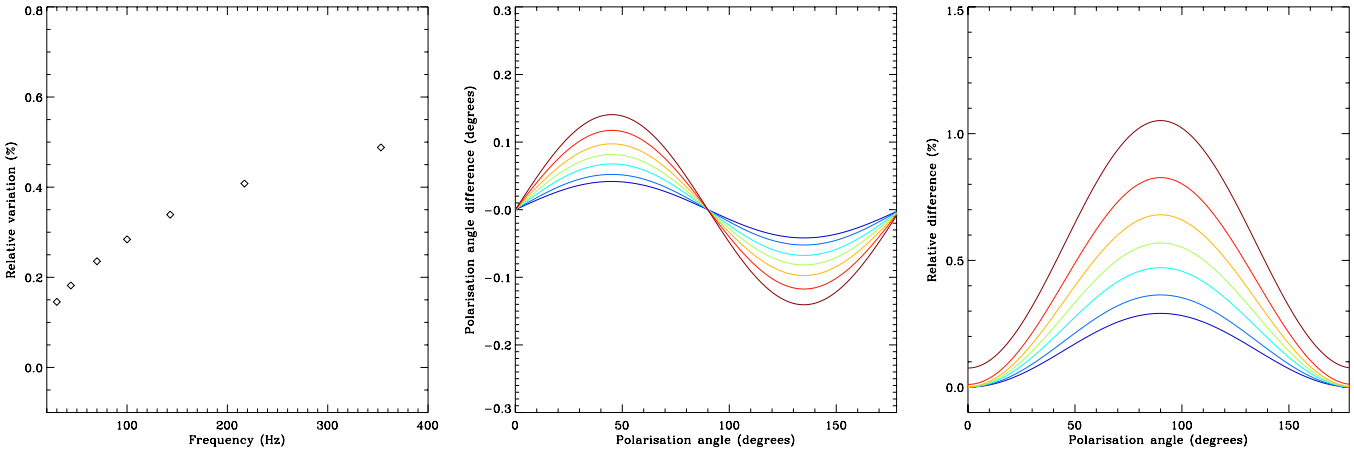

Figure 8. Errors induced in the degree and angle of polarization by an extra low-energy cutoff synchrotron component. Left plot: relative error on the degree of polarization in the case of an unpolarized extra component as a function of the frequency of the polarized *Planck* channels. Middle and right plots: relative error on the degree of polarization and polarization angle error in the case of an extra polarized component as a function of the polarization angle of this component. From blue to red, we represent the values for the different polarized *Planck* channels from 30 to 353 GHz.

(A color version of this figure is available in the online journal.)

the extra synchrotron component is compatible with zero and therefore we conclude that the data show no evidence of an extra synchrotron component.

5. IMPLICATIONS FOR THE *PLANCK* SATELLITE POLARIZATION CALIBRATION

From the previous section, we conclude that the intensity emission of the Crab Nebula at millimeter and submillimeter wavelengths is dominated by the well-known synchrotron radiation observed at radio wavelengths. The data show no evidence of an extra synchrotron component, and evidence for an extra dust component is not significant. Therefore, we can postulate that the Crab Nebula emission at millimeter and submillimeter wavelengths is produced by the same relativistic electrons as those producing the radio emission. Then, it is reasonable to guess that Crab Nebula presents the same polarization properties at radio and millimeter wavelengths. These conclusions are also supported by the Crab polarized emission observed from 23 to 94 GHz by the *WMAP* satellite (Page et al. 2007) when compared to the 363 GHz SCUBA measurements (Greaves et al. 2003) and the 273 GHz data (Flett & Murray 1991). From these, it makes sense to use the low-frequency observations of the Crab Nebula to cross-check and eventually update the knowledge of the polarization characteristics of the high-frequency instruments as proposed by the *Planck* collaboration. As a summary and using the results from Page et al. (2007), Greaves et al. (2003), and Flett & Murray (1991), we expect the Crab Nebula emission at the *Planck* frequencies to be polarized with a degree of polarization of 8%–9% and a polarization angle of 150° in equatorial coordinates (Aumont 2010). Then, at 30 GHz and 353 GHz we expect the total intensity to be 351 ± 7 and 173 ± 5 Jy and the polarized intensity about 28 and 15 Jy, respectively.

However, we can estimate upper limits on the errors induced on the determination of the degree of polarization and polarization angle of the Crab Nebula emission at the *Planck* observation frequencies by the presence of an extra component. For this, we use the results obtained in the previous section and we assume two different cases: polarized and unpolarized extra components. Figure 7 shows 1σ upper limits in the case

of a low-temperature dust extra component. For the left plot, we assume an unpolarized extra component and we present the error on the determination of the degree of polarization as a function of the observation frequency. This error is below 1% for the *Planck* CMB channels from 70 to 217 GHz and rises up to 8% at 353 GHz. The middle and right plots assume a polarized extra component and show the error on the polarization angle and degree of polarization, respectively, as a function of the polarization angle of the extra component with respect to the main synchrotron component. From blue to red, we show the errors from 30 to 353 GHz. The dot-dashed and solid curves assume a degree of polarization of 5% and 10% for the extra component, respectively. As before, the error on the degree of polarization is below 1% at the CMB channels and from 12% to 18% at 353 GHz. For the polarization angle the error is below $0.^{\circ}2$ for the CMB channels and at a maximum of 3° at 353 GHz. Note that the increase in the errors at 353 GHz is mainly due to the large value and large error bars of the Archeops data at 545 GHz and we do not think it is significant. Figure 8 shows the errors induced by an extra LECS component either unpolarized or polarized with a degree of polarization equivalent to the one expected for the canonical synchrotron component. In this case, the errors are much lower being well below 1% and $0.^{\circ}2$ for the degree and angle of polarization, respectively, at all polarized *Planck* frequencies.

6. SUMMARY AND CONCLUSIONS

Within the framework of the polarization calibration of the *Planck* satellite emission, we present in this paper a global analysis of the SED of the Crab Nebula in the frequency range from 1 to 10^6 GHz. For this purpose, we have used new data from the *WMAP* satellite (Page et al. 2007) and from the Archeops balloon experiment (Desert et al. 2008) in addition to data currently available. We focus on the centimetric and millimetric regimes as *Planck* observes the sky from 30 to 857 GHz.

We have first shown that the data are compatible with the canonical model of Crab Nebula emission which assumes a synchrotron component at low and high frequencies, *plus* a dust component at the micrometer wavelengths. To check if an extra component may improve significantly the fit to the data, we consider either an extra LTD emission or an extra LECS component, as in Bandiera et al. (2002). In both cases, we conclude that the current data present no evidence of an extra component. Therefore, the unpolarized millimeter flux of the Crab Nebula is well represented by the following synchrotron power-law model:

$$F_\nu = 973 \pm 19\,\mathrm{Jy}\left(\frac{\nu}{1\,\mathrm{GHz}}\right)^{(-0.296\pm0.006)} \exp\left(\alpha(T_{\mathrm{obs}} - 2003)\right), \quad (1)$$

where $\alpha = -1.67 \times 10^{-3}\,\mathrm{yr}^{-1}$ is the synchrotron fading and ν and T_{obs} are the frequency and the date of observation in years A.C., respectively.

From above, we can conclude that the millimeter emission of the Crab Nebula has the same physical origin as the radio synchrotron emission and therefore it is expected to be polarized with the same degree of polarization and the same orientation. From the current data set, we estimate that the errors on the reconstruction of the degree and angle of polarization on the *Planck* cosmological channels induced by an extra component will be well below 1%. This result strongly supports the choice by the *Planck* collaboration of the Crab Nebula emission for performing polarization cross-checks in the range 30–353 GHz (Aumont 2010).

We thank the Archeops collaboration for their efforts throughout the long campaigns. We acknowledge R. Bandiera and R. D. Davies for very helpful discussions. We finally thank Claudine Tur (LPSC) for fruitful help on bibliographic searches.

REFERENCES

Allen, R. J., & Barrett, A. H. 1967, ApJ, 149, 1
Aller, H. D., & Reynolds, S. P. 1985, ApJ, 293, L73
Aumont, J. 2010, A&A, in press (arXiv:0912.1751)
Baars, J. W. M., et al. 1977, A&A, 61, 99
Bandiera, R., et al. 2002, A&A, 386, 1044
Chini, R., et al. 1984, A&A, 137, 117
Desert, F.-X., et al. 2008, A&A, 481, 411
Dmitrenko, T., et al. 1970, Radiofizika, 13, 823
Flett, A. M., & Murray, A. G. 1991, MNRAS, 249, 4P
Greaves, J. S., et al. 2003, MNRAS, 340, 353
Green, D. A., Tuffs, R. J., & Popescu, C. C. 2004, MNRAS, 355, 1315
Hinshaw, B., et al. 2009, ApJS, 180, 225
Hobbs, R. W., Corbett, H. H., & Santini, N. J. 1968, ApJ, 152, 43
Janssen, M. A., Golden, L. M., & Welch, W. J. 1974, A&A, 33, 373
Kalaghan, P. M., & Wulfsberg, K. N. 1967, Astron. J., 72, 1051
Kellermann, K. I., Pauliny-Toth, I. I. K., & Williams, P. J. S. 1969, ApJ, 157, 1
Kovalenko, A. V., Pynzar', A. V., & Udal'tsov, V. A. 1994, Astron. Rep., 38, 78
Macías-Pérez, J. F., et al. 2007, A&A, 467, 1313
Marsden, P. L., et al. 1984, ApJ, 278, L29
Medd, W. J. 1972, ApJ, 171, 41
Mezger, P. G., et al. 1986, A&A, 167, 145
Page, L., et al. 2007, ApJS, 170, 335
Penzias, A. A., & Wilson, R. W. 1965, ApJ, 142, 1149
Reynolds, S. P., & Chevalier, R. A. 1984, ApJ, 278, 630
Strom, R. G., & Greidanus, H. 1992, Nature, 358, 654
Véron-Cetty, M. P., & Woltjer, L. 1993, A&A, 270, 370
Vinogradova, L. V., et al. 1971, Radiofizika, 14, 157
Vinyajkin, E. N. 2005, ASPC, 342, 435
Werner, M. W., et al. 1977, PASP, 89, 127
Wright, E. L., et al. 1979, Nature, 279, 703
Wrixon, G. T., et al. 1972, ApJ, 174, 399
Zabolotnyi, V. F., Kostenko, V. I., & Slysh, V. I. 1976, Soviet Astron., 19, 405